Origin of the transition voltage in gold–vacuum–gold atomic junctions

Kunlin Wu[1], Meilin Bai[1], Stefano Sanvito[2] and Shimin Hou[1]

[1] Key Laboratory for the Physics and Chemistry of Nanodevices, Department of Electronics, Peking University, Beijing 100871, People's Republic of China
[2] School of Physics and CRANN, Trinity College, Dublin 2, Ireland

The origin and the distance dependence of the transition voltage of gold–vacuum–gold junctions are investigated by employing first-principles quantum transport simulations. Our calculations show that atomic protrusions always exist on the electrode surface of gold–vacuum–gold junctions fabricated using the mechanically controllable break junction (MCBJ) method. The transition voltage of these gold–vacuum–gold junctions with atomically sharp electrodes is determined by the local density of states (LDOS) of the apex gold atom on the electrode surface rather than by the vacuum barrier shape. More specifically, the absolute value of the transition voltage roughly equals the rising edge of the LDOS peak contributed by the 6p atomic orbitals of the gold atoms protruding from the electrode surface, whose local Fermi level is shifted downwards when a bias voltage is applied. Since the LDOS of the apex gold atom depends strongly on the exact shape of the electrode, the transition voltage is sensitive to the variation of the atomic configuration of the junction. For asymmetric junctions, the transition voltage may also change significantly depending on the bias polarity. Considering that the occurrence of the transition voltage requires the electrode distance to be larger than a critical value, the interaction between the two electrodes is actually rather weak. Consequently, the LDOS of the apex gold atom is mainly determined by its local atomic configuration and the transition voltage only depends weakly on the electrode distance as observed in the MCBJ experiments.

1. Introduction

Understanding electron transport at the single molecule level is crucial for the design and the construction of molecular electronic devices [1, 2], which are believed to have the potential of continuing the miniaturization of electronic devices beyond the limits of the conventional silicon-based technology. The current–voltage (I–V) characteristics of molecular devices depend critically on the alignment of the various molecular levels relative to the Fermi level (E_F) of the electrodes. However, this is usually rather difficult to extract both experimentally and theoretically. On the one hand, the energy offset between the electrode E_F and the closest molecular orbital can in principle be obtained directly from the measured I–V curve since a step appears in the current when a molecular level enters the bias window. However, in practice, the relevant molecular levels are often located a few eV away from E_F, so that the junctions are required to withstand a prohibitively large bias without breaking. On the other hand, first-principles density functional theory (DFT) calculations, employing standard local and semi-local exchange and correlation functionals, always predict molecular levels too close to E_F, resulting in an artificially large junction conductance [3].

Recently, Beebe *et al* introduced transition voltage spectroscopy (TVS) as a technique for characterizing

molecular energy levels in molecular devices [4, 5]. In a nutshell, this consists in replotting the I–V data in a Fowler–Nordheim (FN) manner, i.e. as $\ln(I/V^2)$ versus $1/V$. Then a minimum in this plot appears at a characteristic voltage V_{trans}. More interestingly, V_{trans} is found not only to scale linearly with the energy offset between the electrode Fermi level and the highest occupied molecular orbital (HOMO) but also to be much lower than the bias voltage required for resonant tunneling. Hence, TVS is becoming an increasingly popular spectroscopic tool for molecular devices [6–18], and even is extended to characterize gold–vacuum–gold junctions [19]. However, the interpretation of TVS is still under debate [20–25]. It has been argued that the original picture of Beebe *et al*, in which a molecular two-terminal device is treated as a simple tunnel junction such that V_{trans} scales linearly with the barrier height and is independent of the barrier width for a constant barrier height, is not appropriate for molecular junctions [20]. Instead, a coherent Landauer transport model is found to be more appropriate [20] and V_{trans} is related to the applied bias voltage, which promotes a significant tail of the transmission peak into the bias window [21]. Then, it is quite interesting to ask whether gold–vacuum–gold junctions fabricated with the mechanically controllable break junction (MCBJ) method can be described by the standard vacuum tunneling barrier model, considering that this model has been used to describe a variety of metal–vacuum/semiconductor–metal junctions with large transverse extensions for over eighty years [26]. Recently Bâldea demonstrated that even the exact treatment of the standard vacuum barrier model fails at explaining the experimental properties of V_{trans} [27]. Surface states and/or the local density of states (LDOS) of the electrode have been proposed to account for the transition voltage [27, 19], but the origin of surface states and the exact relation between these and the transition voltage is still unknown. Therefore, investigations on the origin and on the properties of the transition voltage in gold–vacuum–gold junctions become an important topic in TVS, since they provide both a test bed for the interpretation of the tunneling mechanism of metal–vacuum–metal junctions with atomically sharp electrodes and an important reference for molecular junctions.

In order to address these questions, we investigate theoretically the electronic transport properties of Au–vacuum–Au junctions. This is realized by employing the non-equilibrium Green's function formalism combined with density functional theory (i.e., the NEGF + DFT approach) [28–37]. Our calculations show that, unlike the zero-bias conductance which is determined by the vacuum barrier shape and thus depends strongly on the electrode distance, the transition voltage of Au–vacuum–Au junctions with atomic protrusions on the electrode surface is mainly determined by the LDOS peak contributed by the 6p atomic orbitals of the apex gold atom. When the electrode distance is large enough to meet the criterion for the occurrence of the transition voltage, the interaction between the two electrodes is rather weak. Thus, the LDOS of the apex Au atom is mainly determined by its local atomic structure and the transition voltage only depends on the electrode distance weakly, in good agreement with the MCBJ experiments [19].

2. Calculation method

In this work we use the SIESTA code [38] to study the atomic structure of Au–vacuum–Au junctions and the quantum transport code SMEAGOL [35–37] to study their electronic transport properties. SIESTA is an efficient DFT package, which adopts a finite range numerical orbital basis set to expand the wave functions of the valence electrons and makes use of improved Troullier–Martins pseudopotentials for the atomic cores [38, 39]. Since basis sets play an important role in the NEGF + DFT calculations [40–44], two different types of basis functions are used for Au atoms respectively in the bulk and at the surface. This allows us to keep a balance between the efficiency and the required accuracy of the simulations. A thorough analysis of the effects of the basis sets on the transport properties of our junctions is given in figure S1 of the supplementary information (available at stacks.iop.org/Nano/24/025203/mmedia). In more detail, a double-zeta basis set augmented with polarization and diffuse functions (DZP + diffuse) is used for the surface Au atoms, while a single-zeta plus polarization (SZP) basis is used for the bulk [45]. We adopt the same cutoff radii for all of the orbitals as those reported by García-Gil *et al* [45], which are optimized to describe accurately the properties of the Au(111) surface. For the DZP + diffuse basis set, the cutoff radii (in Bohr) of each of the orbitals are as follows: 6s (6.52, 4.18), 6p (6.90), 5d (6.18, 2.35) and 7s (9.0). In contrast, for the SZP basis set the cutoff radii of the 6s, 6p and 5d orbitals are 6.52, 6.90 and 6.18 Bohr, respectively. The Perdew–Burke–Ernzerhof (PBE) generalized gradient approximation (GGA) for the exchange and correlation functional is used in all our calculations to account for the electron–electron interactions [46]. Geometry optimization is performed by conjugate gradient relaxation until the forces are smaller than 0.03 eV Å^{-1}.

SMEAGOL is a practical implementation of the NEGF + DFT approach, which uses SIESTA as the DFT platform [35–37]. We use an equivalent cutoff of 200.0 Ryd for the real space grid, while the charge density is integrated over 36 energy points along the semi-circle, 36 energy points along the line in the complex plane, 240 energy points along the real axis, and 36 poles are used for the Fermi function (the electronic temperature is 25 meV). We always consider periodic boundary conditions in the plane transverse to the transport. The unit cell of the extended molecule, for which the self-consistent calculation is performed, comprises some gold atoms with lower coordination and ten Au(111) atomic layers with a (3 × 3) in plane supercell. The I–V curve of the gold–vacuum–gold junctions can be calculated as

$$I = \frac{2e}{h}\int_{-\infty}^{+\infty} T(V,E)[f(E-\mu_{\text{L}}) - f(E-\mu_{\text{R}})]dE, \quad (1)$$

where $T(V,E)$ is the bias V dependent transmission coefficient of the junction, $f(E)$ is the Fermi function, $\mu_{\text{L/R}} = E_{\text{F}} \pm eV/2$ is the local Fermi level of the left/right gold electrode. The zero-bias junction conductance is related to the equilibrium transmission coefficient at the Fermi energy through the Landauer formula $G = \frac{2e^2}{h}T(V=0,E_{\text{F}})$.

Then, the total transmission coefficient $T(V, E)$ of the Au–vacuum–Au junctions is evaluated as

$$T(V, E) = \frac{1}{\Omega_{2DBZ}} \int_{2DBZ} T(\vec{k}; V, E)\, d\vec{k}, \qquad (2)$$

where Ω_{2DBZ} is the area of the two-dimensional Brillouin zone (2DBZ) in the transverse directions. The k-dependent transmission coefficient $T(\vec{k}; V, E)$ is obtained as

$$T(\vec{k}; V, E) = Tr[\Gamma_L G_M^R \Gamma_R G_M^{R+}], \qquad (3)$$

where G_M^R is the retarded Green's function matrix of the extended molecule and $\Gamma_{L(R)}$ is the broadening function matrix describing the interaction of the extended molecule with the left (right) electrode. More details on the method can be found in reference [35–37]. Here, we calculate the transmission coefficient by sampling 4×4 k-points in the transverse 2DBZ.

3. Results and discussion

Considering the fact that a single-atom contact is always formed between the two gold electrodes before the TVS measurements begin [19], two symmetric Au–vacuum–Au junction models are constructed. In these either one gold adatom or a gold cluster with four atoms arranged in a pyramid configuration is attached to the electrode surfaces (figures 1(a) and (f)). For brevity, these two junction models are denoted as Junction–Adatom and Junction–Pyramid. It can be shown that the transmission coefficients at E_F of these two junctions both approach unity when the distance between the two apex gold atoms is kept at about 2.8 Å (see supplement figure S1 available at stacks.iop.org/Nano/24/025203/mmedia). If now the distance between the two apex atoms is set to 6.0 Å, the transmission coefficients at the Fermi level will decrease to 6.9×10^{-3} and 8.9×10^{-3} for Junction–Adatom and Junction–Pyramid, respectively (figures 1(b) and (g)). Below E_F, the transmission is very small because the charge density associated with 5d atomic orbitals of the apex gold atoms decays very quickly into the vacuum; around the Fermi level, the 6s atomic orbital of the apex gold atom dominates its LDOS, thus the transmission is rather smooth. In contrast, transmission peaks appear above the Fermi level. These originate mainly from the 6p atomic orbitals of the apex atoms due to their relatively slow decay in vacuum. Since the interaction between a Au adatom and the Au(111) surface is much stronger than that between the atom at the apex of the pyramid and the Au(111) surface, the transmission peak in Junction–Adatom is much broader than that in Junction–Pyramid and also extends to lower energies.

When a bias voltage is applied, the I–V curve shows a transition from a linear dependence at low voltages to a pronounced nonlinear behavior at large V. As a result, a well-defined minimum appears in the F–N plots of these two junctions (figures 1(d) and (i)), and the V_{trans} values for Junction–Adatom and Junction–Pyramid are respectively determined to be 1.5 and 2.1 V. In both cases these are independent of the bias polarity. Such calculated V_{trans} values are in the range of the measured transition voltages of

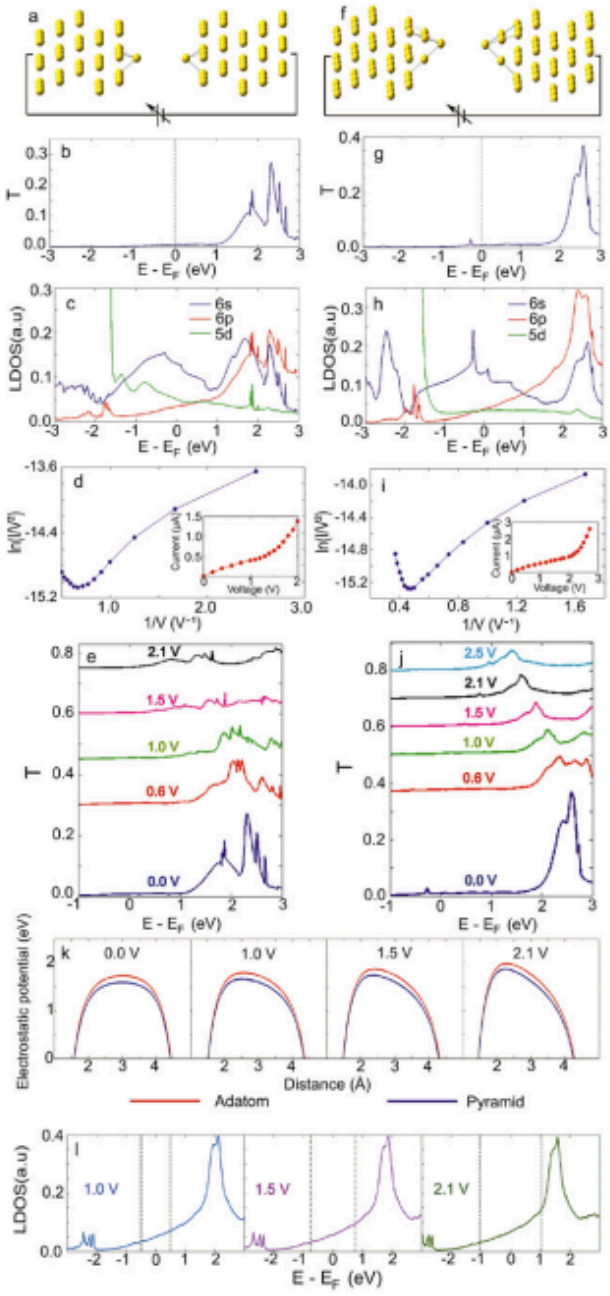

Figure 1. Transport properties and electronic structure of Junction–Adatom and Junction–Pyramid. Optimized atomic structure (a), zero-bias transmission spectrum (b), LDOS corresponding to the gold adatom (c), F–N plot (d) and the bias-dependent transmission spectra (e) of Junction–Adatom. For Junction–Pyramid the same quantities are plotted in panels (f)–(j). In the inserts of panels (d) and (i), the I–V curves of Junction–Adatom and Junction–Pyramid are shown on standard axes. In (k), the bias-dependent electrostatic potentials along a line passing through the two apex gold atoms of Junction–Adatom and Junction–Pyramid are compared. For Junction–Pyramid, the bias-dependent LDOS contributed by the 6p atomic orbitals of the apex gold atom on the electrode whose local Fermi level is shifted downwards are shown in (l), where the two dot lines denote the local Fermi levels.

Au–vacuum–Au junctions [19]. Further understanding can be obtained by plotting the bias-dependent transmission spectra of these two junctions (figures 1(e) and (j)). As we can see, following an increase in the bias voltage, the transmission peak above the Fermi level splits while simultaneously its intensity decreases. Then, the lower peak moves towards the Fermi level continuously and the current through the junction increases rapidly as soon as the peak enters the bias window, i.e., as soon as it moves below the highest of the two electrodes' local chemical potentials. At such bias an inflection appears in the F–N plot. This process is more pronounced in Junction–Pyramid due to the sharpness of its transmission peak. Since the transmission is influenced by both the vacuum barrier shape and the LDOS of the apex atoms, we first plot the bias-dependent electrostatic potentials along a line passing through the two apex atoms (figure 1(k)). As we can see, at each typical bias voltage the overall shape of the electrostatic potentials of the two junctions is very similar and the barrier height of Junction–Adatom is always larger than that of Junction–Pyramid. This clearly disagrees with the result discussed above that the transition voltage of Junction–Adatom is 0.6 V lower than that of Junction–Pyramid, demonstrating that the transition voltage of Au–vacuum–Au junctions with atomic protrusions is not directly related to the vacuum barrier shape.

If we now take a closer look at the LDOS of the apex atoms, we will find that the transition voltage of these two junctions is related closely to the rising edge of the LDOS peak contributed by the 6p atomic orbitals of the apex. Thus, the mechanism of the occurrence of the transition voltage can be described as follows (figure 1(l)). At equilibrium, electrons fill the electronic states up to the Fermi level, thus the 6p states of the apex gold atoms are empty. When a bias voltage is applied, the local Fermi levels of the two electrodes shifts upwards and downwards, respectively (depending on the polarity). Since the interaction between the apex atoms on the two electrode surfaces is rather weak due to the large vacuum gap, the electronic states of the apex shift rigidly with the local Fermi level of the corresponding electrode. When the rising edge of the LDOS peak dominated by the 6p atomic orbitals of the apex corresponding to the electrode shifting downwards aligns with the local Fermi level of the other electrode, the transmission is enhanced significantly and the current through the junction increases rapidly. This leads to the inflection in the F–N plot. Since the energy difference between the local Fermi levels of the two electrodes is just the bias voltage multiplied by the electron charge, the transition voltage of a Au–vacuum–Au junction roughly equals the rising edge of the LDOS peak contributed by the 6p atomic orbitals of the apex located on the electrode shifting downwards in energy. As a result, the transition voltage of symmetric Au–vacuum–Au junctions does not depend on the bias polarity since the LDOS of the two apexes are identical.

In order to further confirm the above analysis, we construct two asymmetric junctions. In the first (figure 2(a)) the surfaces of the two gold electrodes are respectively decorated with a gold adatom and a four-atom gold cluster in the pyramid configuration. The distance between the two apex gold atoms is set to 6.0 Å. In the second (figure 2(d)) only one electrode surface is decorated with a gold adatom, and its distance to the other electrode surface is set to 5.0 Å. These two junction models are denoted as Junction–Adatom–Pyramid and Junction–Adatom–Surface. It can be expected that the transition voltages of these two asymmetric configurations will depend strongly on the bias polarity, because the LDOS of the adatom, the pyramid apex and the Au(111) surface are drastically different (see supplement figure S2 available at stacks.iop.org/Nano/24/025203/mmedia). This is indeed the case.

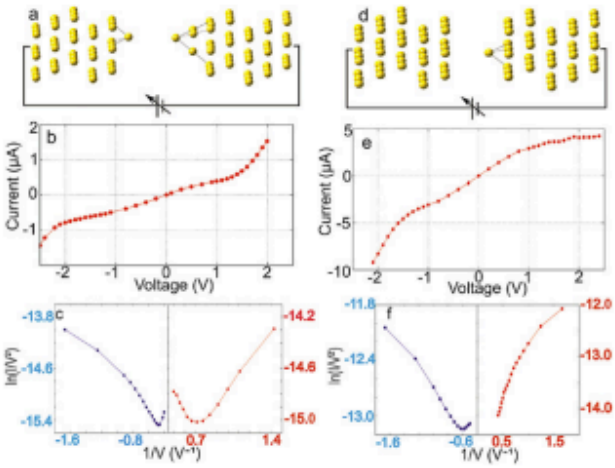

Figure 2. Optimized atomic structure (a), I–V curve on a linear scale (b) and F–N plot (c) of Junction–Adatom–Pyramid. The same quantities for Junction–Adatom–Surface are given in panels (d) through (f).

For Junction–Adatom–Pyramid (figures 2(b) and (c)), when a positive voltage is applied to the electrode containing the gold adatom, the current through the junction increases rapidly as the voltage is increased, and the transition voltage is determined to be 1.5 V, i.e. it is the same as Junction–Adatom with the same electrode distance. In contrast, when the bias polarity is reversed, the increase of the current becomes much slower and the transition voltage increases to 2.1 V. This equal V_{trans} found for the Junction–Pyramid configuration with the same electrode distance. Such a picture is completely consistent with the fact that the LDOS peak contributed by the 6p atomic orbitals of the atom at the pyramid apex is much higher in energy than that of the gold adatom. The situation is even more dramatic for Junction–Adatom–Surface (figures 2(e) and (f)). Although a transition voltage of 1.6 V is obtained when a positive-bias voltage is applied to the electrode with the adatom, the current through the junction increases very slowly up to the bias of 2.4 V and no inflection is observed in the F–N plot when the bias polarity is reversed. The reason for this anomalous behavior is that the LDOS of the gold atoms at the Au (111) surface contributed by their 6p atomic orbitals is very smooth from E_{F} up to 3.0 eV above E_{F} due to their strong interactions with the neighboring atoms. This is also corroborated by the transport properties of a symmetric Au–vacuum–Au junction in which the two electrodes both have an atomically flat (111) surface. Independent of the

bias polarity, the current always increases slowly with the increase of the bias voltage, and no minimum appears in the F–N plot when the bias voltage is increased up to 2.4 V (see supplement figure S2 available at stacks.iop.org/Nano/24/025203/mmedia).

Finally we investigate the dependence of the transition voltage on the distance between the two gold electrodes, by taking Junction–Adatom as a representative example. Figure 3(a) shows the transmission spectra for an electrode distance of 2.8, 3.5, 4.2 and 4.5 Å. We note that, as the distance between the electrodes increases, the transmission peaks around −2.0 eV (dominated by the 5d atomic orbitals) and the transmission coefficient at E_F continuously decrease. In contrast, the change in transmission for energies ranging from 1.5 to 2.8 eV is more complex. Initially and counterintuitively, T(E) in this energy range increases with the electrode distance and the transmission peak centered at the 1.86 eV reaches the maximum of 0.98 at an electrode distance of 4.2 Å. As the two electrodes are moved far from each other the interaction between the two adatoms decreases, thus their 6p orbitals become more localized and generate LDOS peaks in the range 1.5–2.8 eV. Such a LDOS provides a channel for transmission, which consequently gets larger. A further increase of the electrode distance affects only marginally such a LDOS but enlarges significantly the tunneling energy barrier width, such that the transmission in the entire energy range is reduced. Although Junction–Adatom with the electrode distance of 4.2 Å has already shown a pronounced broad transmission peak centered around 2.0 eV above E_F, the current is still unable to increase rapidly enough to satisfy the criterion for the occurrence of the transition voltage, namely that the differential conductance is two times larger than the (pseudo-) Ohmic conductance [27]. This is because the equilibrium transmission coefficient at the Fermi level can reach up to 0.33 and the current at low bias is rather large. When the electrode distance is increased to 4.5 Å, $T(E_F)$ reduces to 0.16, almost half of the value calculated at 4.2 Å. In contrast, the peak value of the transmission at 1.86 eV is still as large as 0.88, nearly 90% of that at the electrode distance of 4.2 Å. As a result, a minimum is observed in the F–N plot of Junction–Adatom with the electrode distance of 4.5 Å and the corresponding transition voltage is determined to be 1.7 V.

The distance dependence of the transition voltage and of $T(E_F)$ for Junction–Adatom is presented in figure 3(b). When the electrode distance is increased from 4.5 to 8.0 Å, $T(E_F)$ reduces from 0.16 to 3.3×10^{-5}, a change of almost three and half orders of magnitude. However, the transition voltage is only changed by 18%, namely it is lowered from 1.7 to 1.4 V. That is, the transition voltage of Junction–Adatom depends only weakly on the electrode distance though a strong distance dependence shows for the transmission coefficient at the Fermi level. Both these facts are in good agreement with experiments [19]. It should be pointed out that similar results are also obtained for Au–vacuum–Au junctions with other geometric shapes. For example, when the electrode distance is increased from 4.8 to 7.0 Å, the transition voltage of Junction–Pyramid decreases from 2.2 to 2.1 V whereas the transmission coefficient at the Fermi level reduces from

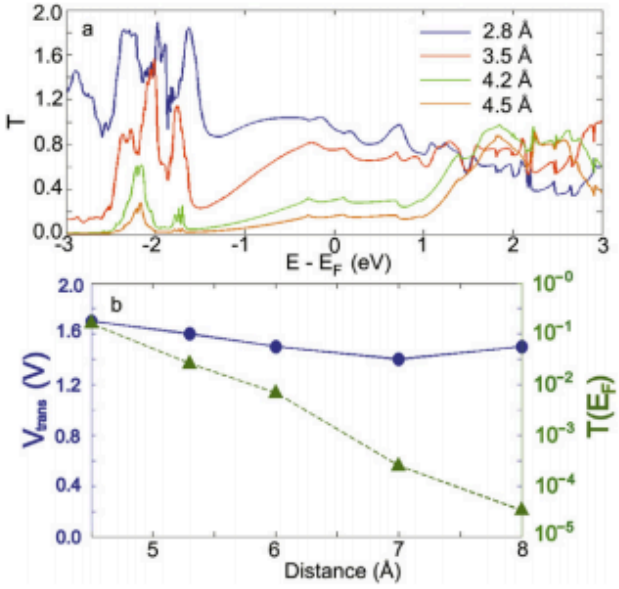

Figure 3. (a) The zero-bias transmission spectra of Junction–Adatom at an electrode distance of 2.8, 3.5, 4.2 and 4.5 Å. (b) The distance dependence of the transition voltage and the transmission coefficient at the Fermi level of Junction–Adatom.

8.3×10^{-2} to 3.9×10^{-4} (see supplementary table S1 available at stacks.iop.org/Nano/24/025203/mmedia). Thus, we can conclude that, in contrast to the zero-bias conductance which is determined by the vacuum barrier shape and thus depends strongly on the electrode distance, the transition voltage of Au–vacuum–Au junctions with atomic protrusions on the electrode surface is determined by the LDOS originating from the 6p atomic orbitals of the apex atom. When the electrode distance is so large that the criterion for the occurrence of the transition voltage is satisfied, the interaction between the two electrodes is rather weak and thus the LDOS of the apex gold atom is mainly determined by its local atomic structure, leading to the weak distance dependence of the transition voltage.

4. Conclusion

We have investigated the origin and the distance dependence of the transition voltage of Au–vacuum–Au junctions using the NEGF + DFT method. Our calculations show that the atomic protrusions, which always exist on the electrode surface of junctions fabricated with the MCBJ method, dominate the transport properties. In particular the transition voltage of gold–vacuum–gold junctions with atomically sharp electrodes is determined by the LDOS of protruding atoms on the electrode surface rather than the vacuum barrier shape. More specifically, the transition voltage is roughly equal to the rising edge of the LDOS peak originating from the 6p orbitals of the apex atom at the surface whose local Fermi level is shifted downwards when a bias voltage is applied. Since the LDOS of the apex atom depends strongly on the exact shape of the electrode, the absolute value of the transition voltage is sensitive to the variation of the atomic

configuration of the junction and, in asymmetric junctions, changes significantly depending on the bias polarity. The occurrence of the transition voltage requires the electrode distance to be larger than a critical value so that the interaction between the two electrodes is rather weak. In this situation the LDOS of the apex atom is mainly determined by its local atomic configuration, which results in the weak distance dependence of the transition voltage as observed in MCBJ experiments.

Acknowledgments

This project was supported by the National Natural Science Foundation of China (No. 61071012) and the MOST of China (Nos 2011CB933001 and 2013CB933404). SS is grateful for additional funding support from the Science Foundation of Ireland (grant no. 07/IN/I945), by KAUST (FIC/2010/08) and by CRANN.

References

[1] Tao N J 2006 *Nature Nanotechnol.* **1** 173
[2] Song H, Reed M A and Lee T 2011 *Adv. Mater.* **23** 1583
[3] Koentopp M, Chang C, Burke K and Car R 2008 *J. Phys.: Condens. Matter* **20** 083203
[4] Beebe J M, Kim B, Gadzuk J W, Frisbie C D and Kushmerick J G 2006 *Phys. Rev. Lett.* **97** 026801
[5] Beebe J M, Kim B, Frisbie C D and Kushmerick J G 2008 *ACS Nano* **2** 827
[6] Liu K, Wang X and Wang F 2008 *ACS Nano* **2** 2315
[7] Pakoulev A V and Burtman V 2009 *J. Phys. Chem.* C **113** 21413
[8] Wang G, Kim T-W, Jo G and Lee T 2009 *J. Am. Chem. Soc.* **131** 5980
[9] Song H, Kim Y, Jang Y H, Jeong H, Reed M A and Lee T 2009 *Nature* 1039
[10] Tan A, Sadat S and Reddy P 2010 *Appl. Phys. Lett.* **96** 013110
[11] Noy G, Ophir A and Selzer Y 2010 *Angew. Chem. Int. Edn* **49** 5734
[12] Bennett N, Xu G, Esdaile L J, Anderson H L, Macdonald J E and Elliott M 2010 *Small* **6** 2604
[13] Choi S H, Risko C, Delgado M C R, Kim B, Brédas J-L and Frisbie C D 2010 *J. Am. Chem. Soc.* **132** 4358
[14] Song H, Kim Y, Jeong H, Reed M A and Lee T 2010 *J. Phys. Chem.* C **114** 20431
[15] Song H, Kim Y, Jeong H, Reed M A and Lee T 2011 *J. Appl. Phys.* **109** 102419
[16] Wang G, Kim Y, Na S-I, Kahng Y H, Ku J, Park S, Jang Y H, Kim D-Y and Lee T 2011 *J. Phys. Chem.* C **115** 17979
[17] Xiang D, Zhang Y, Pyatkov F, Offenhäusser A and Mayer D 2011 *Chem. Commun.* **47** 4760
[18] Guo S, Hihath J, Díez-Pérez I and Tao N 2011 *J. Am. Chem. Soc.* **133** 19189
[19] Trouwborst M L, Martin C A, Smit R H M, Guédon C M, Baart T A, van der Molen S J and van Ruitenbeek J M 2011 *Nano Lett.* **11** 614
[20] Huisman E H, Guédon C M, van Wees B J and van der Molen S J 2009 *Nano Lett.* **9** 3909
[21] Araidai M and Tsukada M 2010 *Phys. Rev.* B **81** 235114
[22] Chen J, Markussen T and Thygesen K S 2010 *Phys. Rev.* B **82** 121412
[23] Markussen T, Chen J and Thygesen K S 2011 *Phys. Rev.* B **83** 155407
[24] Mirjani F, Thijssen J M and van der Molen S J 2011 *Phys. Rev.* B **84** 115402
[25] Bâldea I 2012 *Phys. Rev.* B **85** 035442
[26] Sommerfeld A and Bethe H 1933 Elektronentheorie der Metalle *Handbuch der Physik* vol 24, ed H Geiger and K Scheel (Julius: Springer) p 446 Part 2
[27] Bâldea I 2012 *Europhys. Lett.* **98** 17010
[28] Meir Y and Wingreen N S 1992 *Phys. Rev. Lett.* **68** 2512
[29] Hohenberg P and Kohn W 1964 *Phys. Rev.* **136** B864
[30] Kohn W and Sham L J 1965 *Phys. Rev.* **140** A1133
[31] Xue Y, Datta S and Ratner M A 2002 *Chem. Phys.* **281** 151
[32] Brandbyge M, Mozos J-L, Ordejón P, Taylor J and Stokbro K 2002 *Phys. Rev.* B **65** 165401
[33] Zhang J, Hou S, Li R, Qian Z, Han R, Shen Z, Zhao X and Xue Z 2005 *Nanotechnology* **16** 3057
[34] Li R, Zhang J, Hou S, Qian Z, Shen Z, Zhao X and Xue Z 2007 *Chem. Phys.* **336** 127
[35] Rocha A R, Garcia-Suarez V M, Bailey S W, Lambert C J, Ferrer J and Sanvito S 2005 *Nature Mater.* **4** 335
[36] Rocha A R, García-Suárez V M, Bailey S, Lambert C, Ferrer J and Sanvito S 2006 *Phys. Rev.* B **73** 085414
[37] Rungger I and Sanvito S 2008 *Phys. Rev.* B **78** 035407
[38] Soler J M, Artacho E, Gale J D, García A, Junquera J, Ordejón P and Sánchez-Portal D 2002 *J. Phys.: Condens. Matter* **14** 2745
[39] Troullier N and Martins J 1991 *Phys. Rev.* B **43** 1993
[40] Hou S, Li R, Qian Z, Zhang J, Shen Z, Zhao X and Xue Z 2005 *J. Phys. Chem.* A **109** 8356
[41] Ke S-H, Baranger H U and Yang W 2007 *J. Chem. Phys.* **127** 144107
[42] García Y, San-Sabián E, Louis E and Vergés J A 2008 *Int. J. Quantum Chem.* **108** 1637
[43] Strange M, Kristensen I S, Thygesen K S and Jacobsen K W 2008 *J. Chem. Phys.* **128** 114714
[44] Herrmann C, Solomon G C, Subotnik J E, Mujica V and Ratner M A 2010 *J. Chem. Phys.* **132** 024103
[45] García-Gil S, García A, Lorente N and Ordejón P 2009 *Phys. Rev.* B **79** 075441
[46] Perdew J, Burke K and Ernzerhof M 1996 *Phys. Rev. Lett.* **77** 3865